The theoretical account of the ligand field bonding regime and magnetic anisotropy in the DySc2N@C80 Single Ion Magnet endohedral fullerene

ARTICLE *in* PHYSICAL CHEMISTRY CHEMICAL PHYSICS · APRIL 2014

Impact Factor: 4.49 · DOI: 10.1039/c4cp00953c · Source: PubMed

5 AUTHORS, INCLUDING:

Cimpoesu Fanica
Institute of Physical Chemistry
77 PUBLICATIONS **872** CITATIONS
SEE PROFILE

Nita Dragoe
Université Paris-Sud 11
132 PUBLICATIONS **1,197** CITATIONS
SEE PROFILE

Harry Ramanantoanina
Université de Fribourg
18 PUBLICATIONS **82** CITATIONS
SEE PROFILE

Werner Urland
Université de Fribourg
219 PUBLICATIONS **1,607** CITATIONS
SEE PROFILE

PCCP

PAPER

View Article Online
View Journal | View Issue

Cite this: *Phys. Chem. Chem. Phys.*, 2014, **16**, 11337

The theoretical account of the ligand field bonding regime and magnetic anisotropy in the $DySc_2N@C_{80}$ single ion magnet endohedral fullerene

Fanica Cimpoesu,*[a] Nita Dragoe,[b] Harry Ramanantoanina,[c] Werner Urland[c] and Claude Daul*[c]

Received 5th March 2014,
Accepted 2nd April 2014

DOI: 10.1039/c4cp00953c

www.rsc.org/pccp

Considering the $DySc_2N@C_{80}$ system as a prototype for Single Ion Magnets (SIMs) based on endohedral fullerenes, we present methodological advances and state-of-the art computations analysing the electronic structure and its relationship with the magnetic properties due to the Dy(III) ion. The results of the quantum chemical calculations are quantitatively decrypted in the framework of ligand field (LF) theory, extracting the full parametric sets and interpreting in heuristic key the outcome. An important result is the characterization of the magnetic anisotropy in the ground and excited states, drawing the polar maps of the state-specific magnetization functions that offer a clear visual image of the easy axes and account for the pattern of response to perturbations by the magnetic field applied from different space directions. The state-specific magnetization functions are derivatives with respect to the magnetic field, taken for a given eigenvalue of the computed spectrum. The methodology is based on the exploitation of the data from the black box of the *ab initio* spin–orbit (SO) calculations. The ground state is characterized by the $J_z = \pm 15/2$ quantum numbers with easy axis along the Dy–N bond. The implemented dependence on the magnetic field allowed the first-principles simulation of the magnetic properties. The computational approach to the properties of endohedral fullerenes is an important goal, helping to complement the scarcity of the experimental data on such systems, determined by the limited amount of samples.

Introduction

The physical chemistry of fullerene–lanthanide endohedral complexes occurs at the confluence of two large streams of scientific fundamental interest, on lanthanide[1] and fullerene[2] compounds, each class having rich manifestations, relevant to the quest of finding special properties and potential applications in future technologies. The inclusion of lanthanide atoms inside fullerene cages started with the detection of $La@C_{82}$ in mass spectra (while, initially, no evidence of smaller systems $La@C_{60}$ or $La@C_{70}$).[3] Further evidence by EPR spectra showed that the $La@C_{82}$ system is ionic, with $La^{(3+)}$ and $C_{82}^{(3-)}$ components.[4] Soon after, $Ln@C_{82}$ adducts with many other lanthanide ions (*e.g.* Ln = La, Ce, Pr, Nd, Sm, Gd, Tb, Dy, Ho) were reported.[5] Molecules with two inner lanthanide ions, such as $Ce_2@C_{82}$, were also obtained.[6] Later on, the $Ln@C_{60}$ (*e.g.*, Ln = Eu, Gd, Dy) species appeared.[7] Synchrotron X-ray diffraction, EPR spectra, electrochemical measurements, and ultraviolet photoemission spectroscopy (UPS) data on various $Ln@C_{82}$ species confirmed the trivalent state of lanthanides incorporated into the cage.[8] The above briefing refers to the classical part of fullerenes encapsulating lanthanides story, the further history showing extreme diversification of the encountered species,[9] going up to the recent entries, such as crystallographic resolution of $Yb@C_{80}$,[10] the structural characterization of the series $Sm_2@C_{88}$, $Sm_2@C_{90}$, $Sm_2@C_{92}$,[11] or the $Gd_2@C_{79}N$ hetero-fullerene with a magnetic $S = 15/2$ spin state.[12] A remarkable class is represented by the C_{80} icosahedral cage incorporating a triangle of metal ions, triply bridged by a central nitrogen atom, various $Ln_3N@C_{80}$ systems with trivalent lanthanide ions (Ln = Gd, Tb, Dy, Ho) being investigated.[13] Hetero-metallic compounds with this topology and mixed composition $Ln_xM_{3-x}N@C_{80}$ are also known,[14] an important case being the $DySc_2N@C_{80}$ system,[15] which was revealed with the special Single Ion Magnet (SIM) behaviour, similar to the previously evidenced properties of the Ishikawa's bis(phthalo-cyaninato) lanthanide $[Pc_2Tb]^-$, $[Pc_2Dy]^-$ or $[Pc_2Ho]^-$ mononuclear systems.[16]

[a] *Institute of Physical Chemistry, Splaiul Independentei 202, Bucharest 060021, Romania. E-mail: cfanica@yahoo.com*
[b] *Université Paris Sud, Institut de Chimie Moléculaire et des Matériaux d'Orsay, CNRS UMR 8182, 91405 Orsay Cedex, France*
[c] *Department of Chemistry, University of Fribourg, Chemin du Musée 9, CH 1700 Fribourg, Switzerland. E-mail: claude.daul@unifr.ch*

The SIM property is an astonishing facet of the Single Molecule Magnet (SMM) paradigm,[17] which initially was developed for coordination compounds with large nuclearity[18] and progressively shifted to smaller systems, down to binuclear systems.[19,25b] Although relatively new, the SIM manifestation receives full attention, including illuminating theoretical treatments.[20] The physical chemistry of lanthanide ions inside fullerenes is a new world, yet at the initial stages of exploration, showing promising prospects for a new kind of molecular magnetism, pointing towards the in-vogue topics of the spintronics, as future technology.[21]

Reported calculations devoted to endohedral lanthanide complexes[12,22,23] were confined up to now to the Density Functional Theory (DFT)[24] methods, which, in general, offer reliable information on ground states. However, in the routine computational forms, the DFT approach is incomplete with respect to intrinsic features of lanthanide compounds, such as the multi-configuration nature of the wave functions and the occurrence of quasi-degenerate states.

We enter this topic with a different perspective on the theoretical approach, in response to many open questions to experiment and prospects for special properties due to charge and spin combined effects. We claim pioneering contributions in the *ab initio* multi-configuration wave function[25] and DFT treatment of lanthanide complexes,[26,27] after pointing and solving hidden technical and conceptual problems related to the weakly interacting nature of the f shell. As a consequence of the radial part, contracted inside the atomic body, the f atomic orbitals (AOs) are weakly perturbed by the environment. This sort of electronic structure is problematic in single-determinant methods, like Hartree–Fock of DFT.[25]

In the *ab initio* wave function theory, we resolved the issue going directly into multi-configuration calculations with starting orbitals assembled from fragments, computed individually, in advance, *i.e.* the lanthanide ions and the remainder of the molecule. On the other hand, some of us approached non-routine strategies in the DFT frame, by controlling the orbital occupations[28] or dichotomizing the interaction scheme, keeping only the electrostatic effects.[26] Such procedures, and the subsequent ligand field (LF) analysis, consecrated under the LFDFT acronym,[27] are encompassing limitations of the standard DFT. The LFDFT exploits the subtleties of the conceptual DFT, which allows and assigns a clear physical meaning to the systems with fractional spin and orbital populations.[29] This kind of non-standard approach is possible only in certain computing packages, such as the ADF (Amsterdam Density Functional) code,[30] which is appropriate to the given problems by interesting leverages, such as working with fragments or treating the electrostatics of the environment under the so-called Frozen Density Embedding (FDE).[31]

Results and discussion

Molecular geometry and general bonding features

Before entering the main issue of the *ab initio* account of the specifics due to the f shell in the electron structure and magnetic properties of the $DySc_2N@C_{80}$ system,[15] we will consider the preamble of the general structural description. Since the overall geometry of the molecule can be properly perceived from the following pictures, dedicated to the molecular orbitals, or from the figures of the other works,[13–15] we will start with the idealized view from Scheme 1, based on the results of geometry optimization by DFT.

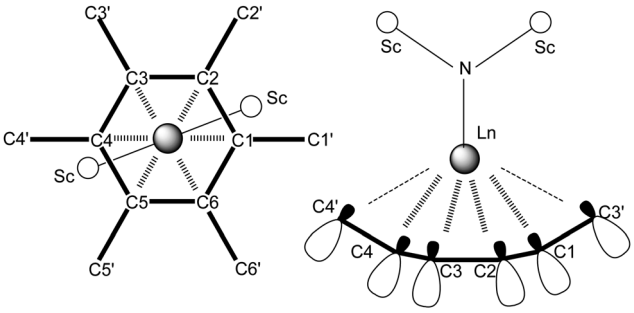

Scheme 1

We used, along with the optimization procedure, the facility of ADF code to work with Average of Configuration (AOC), smearing the nine electrons from the f^9 configuration of Dy(III) over seven MOs having predominant f character (*i.e.* having the 9/7 = 1.2857 population). Recalling that fractional occupations are allowed in DFT,[29] we point that this non-standard option improves the convergence and leads to a reference with a convenient physical meaning, mimicking the barycentre of the f orbital split. Since the f-type LF gap is expected in the order 10^2–10^3 cm^{-1}, *i.e.* negligible in the scale of molecular bonding and thermochemical effects, this conventional choice does not impinge upon the quality of the geometry optimization itself. The optimization can be done, in principle, without this constraint, but leads to doubly occupied f-type orbitals smeared in small fractions among the ligand-type MOs and distant in energy from the single occupied f-type MOs, if the calculation is of restricted type. If the unrestricted way is followed, the f orbitals from α and β sets are, after convergence, separated by large gaps, the situation being inappropriate for LF considerations. The AOC option is a rational manner to conduct calculations that are further devoted to the f-shell LF problems.

The optimized Dy–N bond length is 2.225 Å, sensibly shorter than the usual coordination bonds in lanthanide complexes. For instance, in the $[Pc_2Ln]^{(-)}$ units, the average Ln–N distances are about 2.38 Å.[32] It seems then that the $DySc_2N$ moiety is constrained to compressed bond lengths inside the fullerene cage. In an approximate description, suggested in Scheme 1, the N–Ln bond points towards the middle of a hexagonal face of the C_{80} cage, the corresponding C1–C6 carbon atoms forming the first environment. The atoms labelled C1′–C6′ form a second layer, able to exert LF perturbation to the lanthanide ion. The whole system has C_2 symmetry, for instance the Ln–C1 and Ln–C4 bonds being equivalent. Mentioning only the symmetry independent coordination contacts, the following bond lengths were obtained by DFT optimization: R(Dy–C1) = 2.577 Å, R(Dy–C2) = 2.573 Å and R(Dy–C3) = 2.577 Å, for the closest

contacts, while R(Dy–C1′) = 2.954 Å, R(Dy–C2′) = 2.986 Å and R(Dy–C3′) = 2.957 Å for the distant neighbours. Qualitatively, the system can be characterized by an effective strong axial character, given the short bond with the nitrogen atom *vs.* the larger distances to the carbon cage. Since the electron density is mainly located on the external surface of the fullerene, as suggested in the right side of the Scheme 1, the inward perturbations due to the carbon atoms can be thought to be relatively small. In an intuitive explanation, the flattened pyramidal pattern of the carbon atoms environment on the fullerene surface determines hybrid lobes oriented outside the cage. Then, the LF perturbation is exerted by the small lobes pointing inside. The general bonding regime of the inserted cluster can be characterized as similar to the organometallic lanthanide complexes.

The *ab initio* ligand field modelling of $LnSc_2N@C_{80}$ systems

In the following we will use the Complete Active Space Self Consistent (CASSCF) procedures. Given the weakly interacting nature of f electrons, our strategy of using a starting function produced by merging orbitals from preliminary calculations of the free lanthanide ions and remainder of molecule is an appropriate way. This methodology is conveniently handled with files from the GAMESS code.[33] For problems implying the f shell, the second order perturbation (PT2) procedures, in their various implementations[34,35] are in fact not of strong relevance. We earlier probed[25] that in the lanthanide complexes the CASSCF calculations imply small PT2 increments, which do not alter basic quantities and underlying mechanisms. This is because the PT2 terms are conceived to alleviate the limited choice of active space, when MOs that may be relevant for the investigated effects are left outside. However, this is not the case in the lanthanide systems, where an active space reflecting the f^n configuration describes well the physics related to the LF pattern and the molecular magnetism.

The effective core potential (ECP) type basis sets, particularly the Stevens–Basch–Krauss–Jasien–Cundari (SBKJC)[36] used here, give good results in quantum chemistry of lanthanide complexes. First of all, this is proved by our previous works which, in the CASSCF/SBKJC setting, retrieved in several instances the *ab initio* magnetic computed properties in line with the experimental data.[25,37]

We present in the following assessments justifying the reasonability of the used setting. A clear test is done by briefly mentioning results obtained on the well-known Ishikawa's compounds, for which reliable experimental ligand field parameters are known.[16a,b] Such systems can be idealized to D_{4d} symmetry, the LF problem being expressed by only three parameters: $A_{2,0}\langle r^2\rangle$, $A_{4,0}\langle r^4\rangle$, $A_{6,0}\langle r^6\rangle$. Without entering details, the CASSCF/SBKJC approach of the $[Pc_2Tb]^-$ phthalo-cyaninato complex yielded for the above enumerated parameter set the respective {433.8, −173.7, 37.2} values (in cm^{-1}), matching fairly well the corresponding {414.4, −227.5, 33.5} fit to the experiment. In this test, we used the 6-311G* basis for N and 6-31G for C and H, while the geometry was obtained from DFT optimization. Using a multi-reference second order perturbation scheme implemented in the GAMESS code[33] we obtain the {536.7, −149.4, 40.7} values, in cm^{-1}. The result is, however, sensitive to various technical details, such as choosing between Nakano's quasi-degenerate perturbation code[34c] and Ivanic's[38] determinant-based methods, or even to slight changes in the orbital set produced by doing the calculation within different subgroups of the D_{4d} symmetry, in some cases obtaining large over-estimations of the LF parameters. Such instabilities are due not to code errors, but to the fact that the PT2 schemes themselves are dependent on conventional choices. The amendment of the CASSCF/SBKJC results by the N-electron valence perturbation theory (NEVPT2),[35] as implemented in the ORCA program,[39] which seems a stable version of PT2, yielded the {446.6, −147.4, 36.4} (cm^{-1}) parametric set, supporting our point that the second order perturbation treatments do not bring essential corrections to the computed LF scheme of the f ions. It seems that the CASSCF level is sufficient in numerical sense and, in this circumstance, recommendable in conceptual respects, because the variational nature of the wave function ensures the hold of several basic theorems of electronic structure, while the second order perturbation solutions are yet prone to different conventions that can change the quantitative outcome and the underlying interpretation.

Another issue concerns the basis set of the lanthanide ion, which we claim that for the f-type LF account is not necessary to be very rich in primitives, once the basic profile of the f radial part is well accounted. Using the SARC-ZORA full electron basis set,[40] on the mentioned $[Pc_2Tb]^-$ probe, we get for the {$A_{2,0}\langle r^2\rangle$, $A_{4,0}\langle r^4\rangle$, $A_{6,0}\langle r^6\rangle$} parameters the {328.2, −154.4, 35.1} values (in cm^{-1}), which underestimate the magnitude, in comparison to the experimental set. It is not our purpose to investigate all the possible tunings of technical ingredients, confining ourselves to an apparently modest choice of basis sets which, however, is proved to work well.

As recognized earlier,[41] the f-orbitals are spatially contracted inside the atomic body, having the peak of radial function of the f shell at about 1.2–1.4 Å, sensibly smaller than the atomic radii, which vary between 1.74 Å (at Lu) to 1.87 Å (at La). In this circumstance, the basis set of coordination atoms does not affect much the pattern of the ligand field, since the weak overlap is governed by the main profile of a ligand donor function, not depending much on details due to the decoration with small tails of many primitives, such as extra-polarization components. Even though the bonding regime in lanthanide complexes is not purely ionic, it has such a large character and the significant potential integrals that provoke the LF effects are mainly accounted for with rather modest basis sets on the ligand.

In principle, we agree that the complete basis sets are better than effective potential ones, but since the lanthanide chemistry is confined to the f-shell, a good radial shape of these functions is sufficient, irrespective of the other constituents of the atomic bodies. The other basis set components may be important in accounting other general features, like thermochemistry, but with respect of the LF issues, the quality of the f pattern is the fact that matters essentially. We add these notes as methodological

sidewise of our work. We consider the noted aspects as an encouraging message for a wider approach of quantum chemistry of lanthanide complexes.

Thus, for mono-nuclear lanthanide complexes, the CASSCF(7, *n*) procedures (ascribing the case of *n* electrons in 7 orbitals) give a reasonable and realistic account of the LF phenomenology. Aside the system of interest, $DySc_2N@C_{80}$,[15] we added in the actual computation experiments the $TbSc_2N@C_{80}$ congener (taken at the molecular geometry of Dy case, for comparison reasons).

The calculation on the terbium system was done using a CASSCF(7, 8) procedure, *i.e.* 8 electrons in 7 orbitals, corresponding to the f^8 configuration, averaging over the seven roots related to the ^7F ground term. Similarly, the Dy case implied CASSCF(7, 9) calculations, averaging over 11 roots originating from the LF split of the ^6H term. The results are presented in Table 1, comparing the use of the 6-31G *vs.* 6-31G* basis sets, which are concluded closely similar, for each lanthanide compound. This proves that the calculations on lanthanide systems do not demand a high setting, with rich basis sets on the whole molecule.

The terbium complex is a useful numerical experiment, offering a direct view of the LF strength, since the split of the atomic term ^7F parallels the phenomenological ligand field scheme. Running the β electron of the f^8 configuration (or, in other words, the doubly occupied function) on the seven f-type MOs, one obtains a simple basis for the ^7F term. This problem shows one-electron effective nature. The total gap computed on the terbium complex (see Table 1), of about 1300 cm^{-1}, indicates a strong ligand field. The values usually encountered in f-complexes are in the 500–800 cm^{-1} range.[42]

The short Ln–N bond, discussed previously, can be inferred as the reason for the large LF strength. This fact is proved by performing numerical experiments with CASSCF calculations on the $[TbNSc_2]^{(6+)}$ and $[Tb@C_{80}]^{(3-)}$ complexes, testing the ligand field exerted by the individual ligands: the nitride from the central fragment and the fullerene cage. Even though in the formal ligand field theory the donor perturbations can be assumed additive,[43] in realistic systems, due to the implication of charge and polarization effects, the transferability of LF parameters is not completely presumable. However, we found, interestingly, that the total LF split of the $TbSc_2N@C_{80}$ system is roughly approximated as the sum of the total gaps computed for the above mentioned fragments. Thus, the $[TbNSc_2]^{(6+)}$ case yields the {0.0, 2.3, 234.0, 281.3, 639.0, 879.5, 1102.3} series of values, in cm^{-1}, while the calculation on $[Tb@C_{80}]^{(3-)}$ (confined to the use of 6-31G basis set on carbon atoms) produced the following levels: {0.0, 109.0, 143.8, 161.1, 189.8, 296.3, 325.6} cm^{-1}. The sum of the total gaps is about 1400 cm^{-1}, relatively well related to the 1300 cm^{-1} split in the $TbSc_2N@C_{80}$ system.

The multi-reference perturbation treatment from the GAMESS environment leads to values that seem flawed by the alleged general sensibility of second order increments to the orbital set, yielding the following levels: 0, 1031.9, 1174.9, 1773.9, 2410.1, 2622.7, 2710.6 (in cm^{-1}). This is clearly an unbalanced description, enhancing about two times the total gap, while about ten times the space between the ground and first excited states. For alternate estimation, we turned to ORCA program,[39] using the NEVPT2 method,[35] that leads for the system with Tb/SBKJC, (Sc,N)/6-31G* and C/6-31G to the following values of the ^7F split: 0, 99.9, 521.6, 630.0, 1212.9, 1391.8, 1426.0, in cm^{-1}. The CASSCF step gave the same result as the GAMESS run. One may note the relative minor correction brought about by the second order treatment, in line with our previously expressed reasoning. The calculation with the above mentioned basis set, working on four processors, took one day, while the attempt to do the second order treatment on the system with 6-31G* basis on C atoms was not yet ended within a month. We worked on four processors, in order to keep the total memory in the available range. Richer basis sets and PT2 treatment become prohibitive for a molecule at this scale, but we provided reasons and comparisons advocating that these ingredients are not really necessary for an f-shell LF problem.

As mentioned previously, we generally use the strategy of merged fragment orbitals. Alternatively, another route of guess is possible, taking the unrestricted natural orbitals (UNOs) from DFT calculations, which in lanthanide cases should retrieve components with main f character. We probed that rich lanthanide basis sets may face difficulties in the UNO guess approach, due to spurious mixing of components, in some circumstances, *e.g.* a metal–ligand bond shorter than usual range, as is the case of our nitride ligand.

It is interesting to look at the canonical orbitals of the $DySc_2N@C_{80}$ molecule. The shape and ordering is similar for the terbium congener, the qualitative aspect being, as well, independent from the basis set.

One observes that the shapes of the MOs are similar to the pure f-orbitals in the axial symmetry definition, the approximate ordering being assignable to the $\{xyz, z(x^2 - y^2)\}$, $\{x(x^2 - 3y^2), y(3x^2 - y^2)\}$, z^3, $\{xz^2, yz^2\}$ list. In other words, using the projection $m \equiv l_z$ values, the ordering of the MOs formally follows the $\{\pm3, \pm2, 0, \pm1\}$ sequence, or the $\{\varphi, \delta, \sigma, \pi\}$ symmetry labelling in the $D_{\infty h}$ point group. The axial nature is here only an effective idealization, supported by the visual aspect of the MOs. Besides, the wavefunction of the reported CASSCF calculations on the $TbSc_2N@C_{80}$ system can be approximated as the run over the doubly occupied components of the f^8 configuration, successively

Table 1 The results of CASSCF calculations on the $LnSc_2N@C_{80}$ complexes, simulating the LF split of the ^7F term for Ln = Tb and of the ^6H term for the Ln = Dy, using two different basis sets (6-31G and 6-31G*) on fullerene fragment (while 6-31G* on Sc_2N and SBKJC on Ln)

Ln	Tb	Tb	Dy	Dy
C basis set	6-31G	6-31G*	6-31G	6-31G*
1	0.0	0.0	0.0	0.0
2	91.5	85.7	2.0	1.8
3	454.5	467.4	787.4	797.6
4	508.1	520.0	792.2	801.8
5	1219.1	1260.1	919.3	952.7
6	1239.4	1263.7	978.1	1007.6
7	1285.9	1306.1	1113.3	1147.2
8			1138.5	1172.2
9			1242.1	1269.5
10			1350.9	1378.0
11			1363.9	1388.4

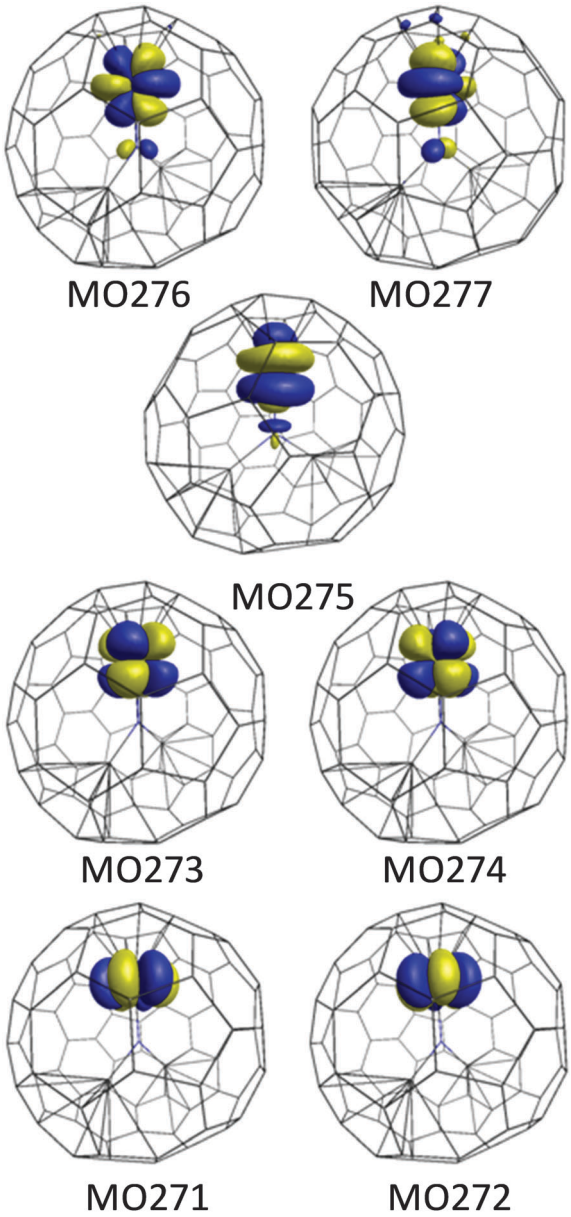

Fig. 1 Canonical molecular orbitals from the CASSCF(7, 9) calculations on the $DySc_2N@C_{80}$ system. The labels correspond to the order number in the MO list.

over the orbitals labelled as MO271–MO277 in Fig. 1. In principle, each eigen-state is a combination of the seven Slater determinants, but, in this case one MO configuration has preponderance in a given CASSCF state. For instance, the ground state consists mostly of the double occupation of the MO271 orbital, and so on. This fact supports the above mentioned approximated {φ, δ, σ, π} sequence in the LF split of the encapsulated lanthanide ion, even tough, as can be seen from the values in the first or second columns of Table 1, the degeneracy of the inferred couples is not perfect.

The shape of the canonical MOs resulted from the calculations with the separated ligands can be idealized as in Scheme 2 for the $[TbNSc_2]^{(6+)}$ unit and like in Scheme 3 for the $[Tb@C_{80}]^{(3-)}$ fragment.

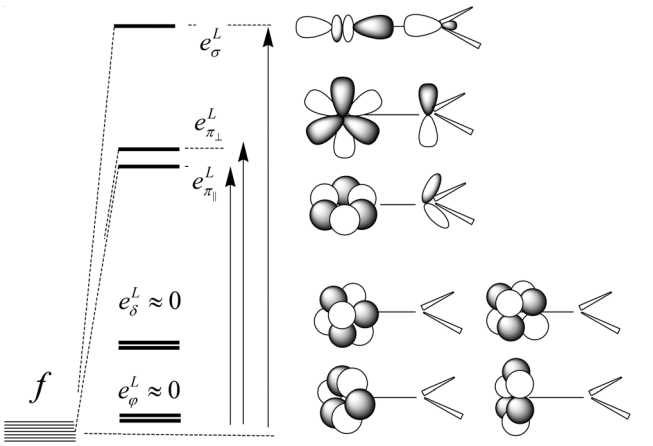

Scheme 2

For the first case, the diagram is in line with the concepts of the Angular Overlap Model (AOM) adapted to the f shell[44,45] (Scheme 2). Thus, the most perturbed orbital is those assigned to the σ component, the z^3 AO pointing the lobe directly to the ligand. Having the Sc_2N triangle located in the *xz* plane, the yz^2 orbital, perpendicular to the ligand plane, is labelled by $\pi_\perp$, interacting with a π-type ligand orbital. Its companion, xz^2, labelled $\pi_\parallel$, interacts with an asymmetric combination of bond orbitals.

Looking carefully at magnified portions of the orbitals from the top of Fig. 1, one observes the small tails corresponding to the mentioned σ lone pair (MO275), the $\pi_\perp$ (MO276) and $\pi_\parallel$ (MO277) ligand components. This supports the idea of a conceptual AOM perspective on the lanthanide ligand field. The other components show no visible ligand tail, since the δ and φ symmetries are not "natural" bonding components of the ligands based on atoms from the second row of the periodic table. However, distinct perturbation of δ and φ type can result just from electrostatic or other intricate exchange–correlation effects, instead of the orbital overlap.

Having a {φ, δ, π, σ} approximate sequence, the $[TbNSc_2]^{(6+)}$ fragment shows a regular AOM-type scheme, where the higher position is correlated with the stronger metal–ligand overlapping. In fact, the combination suggested in Scheme 2 and visible in the MOs from Fig. 1 corresponds to anti-bonding relationships, the metal *vs.* ligand lobes facing each other with different signs.

The qualitative diagram of the ligand field exerted by the fullerene fragment follows a different pattern (Scheme 3), suggesting the {σ, δ, φ, π} irregular ordering. This is because the fullerene, acting with the proximal ring of carbon atoms placed at about 2.4 Å and the next shell of atoms at about 2.9 Å does not behave as a normal linearly ligating system, even preserving the linear-type symmetry labelling. Thus, contrary to normal ligands, where the σ type component is the highest, here is the lowest, since the z^3 AO lobe points towards the void of the hexagonal ring, being less perturbed.

The π-type f orbitals are the highest in the qualitative scheme (abstracted from approximating and extrapolating facts from *ab initio* calculation of the $[Tb@C_{80}]^{(3-)}$ test molecule),

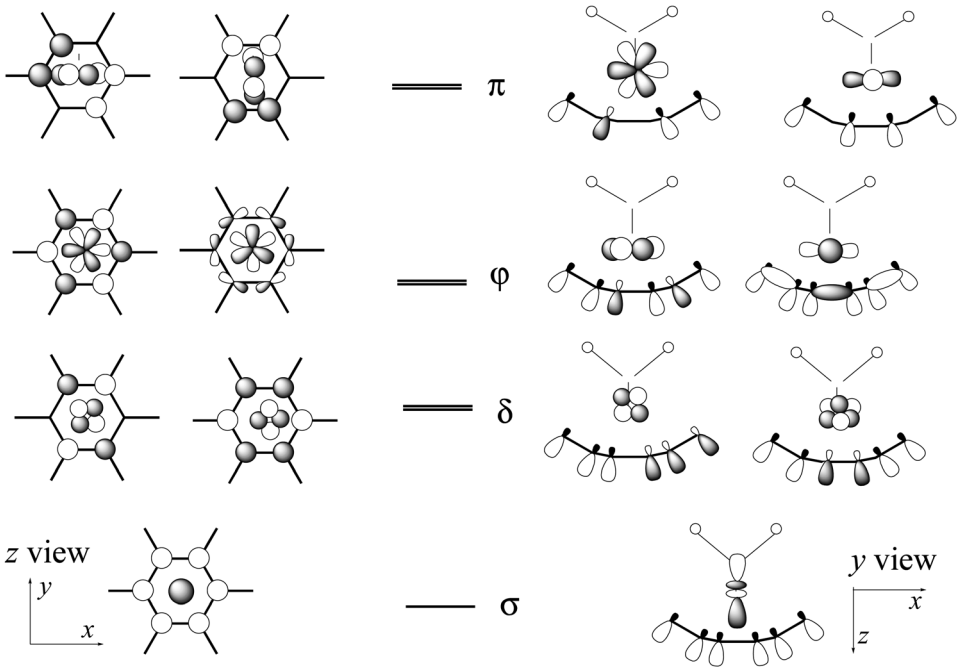

Scheme 3

because their lobes intercept well the orbitals located on the fullerene surface. The φ orbitals seem to be appropriate to meet the lobes from the next neighbouring ring of the carbon atom, due to the curvature of the fullerene surface. The superposition between the different trends exerted by the $\{NSc_2\}$ and $\{C_{80}\}$ ligands leads to the LF diagram suggested by the MOs from Fig. 1. Thus, the z^3 is highest in the strong perturbation due to the single nitride ligand, while lowest in the overall perturbation due to the carbon atoms, which individually have small coordination strength, but are sizeable in the concerted cumulative effect, the resultant being the intermediate position of the z^3, as visible in Fig. 1. One may note that the π type MOs are higher in the LF diagram qualitatively extrapolated from Fig. 1, cumulating the common trends sketched in Schemes 2 and 3, namely having high energy position in both diagrams.

The complete LF modelling is done by analysing the *ab initio* CASSCF full Hamiltonian matrices, by fit to the phenomenological Hamiltonian ascribed in the classical form (see equation 2.7 in ref. 42):

$$\hat{H}_{\mathrm{LF}} = \sum_{k=2,4,6}\sum_{q>0}^{k}\sqrt{\frac{4\pi}{2k+1}}\Big[B_q^k\big(Y_{k,q}+(-1)^q Y_{k,-q}\big) + iB_{-q}^k\big(Y_{k,-q}-(-1)^q Y_{k,q}\big)\Big] + \sum_{k=2,4,6}\sqrt{\frac{4\pi}{2k+1}}B_0^k Y_{k,0}. \quad (1)$$

Since the definition of the B_q^k parameters may vary with respect to particular convention (here using the real numbers format called Wybourne parameterization),[46] we further convert them into the so-called normalized Stevens parameters, $A_{k,q}\langle r^k\rangle$,[47] with the following rescaling:

$$A_{k,q}\langle r^k\rangle = \lambda_{k,q}B_q^k, \quad (2)$$

the $\lambda_{k,q}$ normalization coefficients being found, for instance, in Table 2.2 from Newman's handbook.[42]

Even though the MOs obtained from the calculations are qualitatively close to pure f basis, to rigorously apply the LF analysis, we had to handle in a non-routine manner the results of the CASSCF calculations. In short, the stages are: (i) take canonical MOs and perform a unitary transformation that produces new MOs as close as possible to standard pure f-AOs; (ii) do a configuration interaction (CI) calculation with the new orbitals (since a unitary transformation does not affect the CASSCF states, the results have the same eigenvalues, while different eigenvectors); (iii) collect the CI eigenvalues and eigenvectors and do the back-transformation that retrieves the *ab initio* Hamiltonian matrix (before diagonalization). The GAMESS[33] environment is convenient for such operations.

The retrieved *ab initio* Hamiltonian blocks (with 7×7 size in the case of terbium complex – corresponding to the ^{7}F term, and 21×21 for dysprosium case – containing the ^{6}H and ^{6}F terms) are fitted to the analytical expressions of the LF Hamiltonian matrices. The non-diagonal elements, accounted in this way, play a non-trivial role in the identification of the many LF parameters encountered in the general case of low symmetry. Since each matrix element is developed as a linear expression of the LF parameters and Slater–Condon two-electron terms (which can be discarded in Tb case being the same for all the diagonal elements of the ^{7}F matrix), the fitting problem results in a stack of least-square linear equations that have a unique solution, avoiding in this way problems related to local accidental minima from the general optimization problems. Table 2 shows the LF fit to the *ab initio* results. One notes that the basis set does not impinge much on the scheme, and that the Tb and Dy are approximately comparable.

Table 2 The $A_{k,q}\langle r^k\rangle$ ligand field parameters (in cm^{-1}) resulted from the LF analysis of the *ab initio* computed ground state multiplets for the $LnSc_2NC_{80}$ (Ln = Tb, Dy) systems, considering two types of basis sets on the fullerene cage

Ln	Tb	Tb	Dy	Dy
Basis set on C	6-31G	6-31G*	6-31G	6-31G*
$A_{2,-2}\langle r^2\rangle$	−40.5	−45.2	0.0	0.0
$A_{2,0}\langle r^2\rangle$	1065.0	1095.1	1321.0	1346.0
$A_{2,2}\langle r^2\rangle$	−164.4	−126.1	−148.1	−149.9
$A_{4,-4}\langle r^4\rangle$	−38.5	−45.0	0.0	0.0
$A_{4,-2}\langle r^4\rangle$	7.5	11.1	−0.9	−1.3
$A_{4,0}\langle r^4\rangle$	86.3	90.1	88.8	91.8
$A_{4,2}\langle r^4\rangle$	−18.9	11.7	12.0	14.0
$A_{4,4}\langle r^4\rangle$	25.0	22.9	19.8	17.9
$A_{6,-6}\langle r^6\rangle$	123.3	114.4	112.3	103.2
$A_{6,-4}\langle r^6\rangle$	78.9	87.8	83.1	81.0
$A_{6,-2}\langle r^6\rangle$	−31.4	−29.1	−38.9	−37.8
$A_{6,0}\langle r^6\rangle$	−46.2	−44.1	−46.1	−43.7
$A_{6,2}\langle r^6\rangle$	96.6	106.5	109.4	108.4
$A_{6,4}\langle r^6\rangle$	−48.4	−44.0	−41.4	−40.5
$A_{6,6}\langle r^6\rangle$	19.4	17.9	16.4	14.9

One observes the absolute domination of the $A_{2,0}\langle r^2\rangle$ term that leads to the effective axial appearance of the LF scheme. The parameters with odd q indices vanish due to the C_2 symmetry.

Since the $A_{k,q}\langle r^k\rangle$ parameters themselves are not very transparent to the intuition, we offer in Fig. 2 a picturesque perspective on the LF: the colour map of eqn (1) after using, *via* eqn (2), the values from Table 2.

One clearly observes the quasi-axial pattern. The red areas placed at poles represent the zones of high LF strength. The low LF zone can be described, in analogy to earth globe, as extended between the north and south tropics, namely the portion where only distant carbon atoms from the fullerene cage are projected on the coordination sphere.

We point out that the LF modelling (either based on Spherical Harmonics expansion, like in eqn (1), or the AOM type) undergoes the so-called holohedrization effect.[48] Namely, the perturbations coming from opposed directions of the space, let us say, due to A and B different *trans* ligands, cannot be discriminated individually, the equations describing an artificial form, similar to the hypothetical (A + B)/2 smeared perturbation, equally distributed at sides of the given axis. This is because, for each element, the f × f ligand field matrix has $u \times u = g$ symmetric parity and cannot account for terms with asymmetric u pattern. Or, in other words, the LF Hamiltonian from (1) is based only on even k = 2, 4, 6 Spherical Harmonics, enforcing the inversion symmetry. It follows that the observed axial LF map, symmetric on both sides, towards NSc_2 and fullerene, is also due to the limitation of the LF Hamiltonian to account for a certain polarization due to different perturbation strengths of the A = nitride and B = fullerene wall, producing in each direction of the z axis the averaged (A + B)/2 effect. The *ab initio* matrices contain the odd components that are not accounted in the LF formalism, the MOs showing, *e.g.*, small portions of d-type AOs. At the same time, the asymmetry due to odd terms is not extreme. If these odd terms played an overwhelming role, then the shape of canonical MOs would result visible asymmetric, *e.g.* by d–f hybridization, which seems not to be the case.

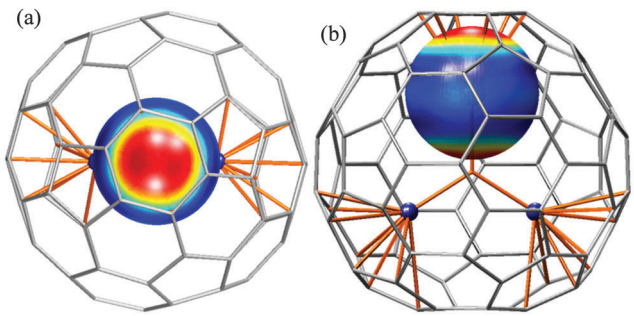

Fig. 2 The polar map of the LF potential drawn as colour scaling (red = high field, blue = low field) with values fitted to the Hamiltonian matrices of the CASSCF(7, 8)/(Tb/SBKJC) (C, N, Sc/6-31G*) calculations on the $TbSc_2N@C_{80}$. (a) View along N–Ln axis, (b) view perpendicular to the N–Ln axis and NSc_2 plane. The other calculations (changing the basis set and the lanthanide ion) give results with similar aspect.

Magnetic anisotropy in the $DySc_2N@C_{80}$ single ion magnet

In the above numerical experiments, we intentionally avoided to introduce the spin–orbit (SO) coupling in the calculations, in order to discriminate the pure LF factors. It is well known that the physics of lanthanides is governed by the SO splitting that supersedes in magnitude the LF effects.[42] The results of the CASSCF-SO calculations are summarized in Table 3, presenting the lowest levels related to the split ground J multiplets (J = 6 for Tb and J = 15/2 for Dy).

One notes that the dysprosium system shows couples with rigorous double degeneracy, due to Kramers symmetry from the half integer J quantum number. The terbium case shows quasi-degenerate pairs in the lowest part of the spectrum and progressively separated lines in the upper part. The averaged spin–orbit coupling constant for the dysprosium case, taken in the $\lambda\hat{L}\cdot\hat{S}$ phenomenology, is estimated at about $\lambda = -2074\ cm^{-1}$.

We will concentrate now on the $DySc_2NC_{80}$ system. A very suggestive manner to discuss the anisotropy, presented by us in previous works,[37] consists of producing the polar maps from the derivatives of eigenvalues of the *ab initio* CASSCF-SO Hamiltonian, with respect to the magnetic field. Scanning the direction of the field derivative, as a function of the θ, φ polar coordinates, one obtains for each "i" state a function:

$$M_i(\theta,\varphi) = -(\mathrm{d}E_i/\mathrm{d}B)_{\theta,\varphi}, \quad (3)$$

called state-specific magnetization. The macroscopic magnetization is a statistics over such components. The polar maps for the states of the discussed system are shown in Fig. 3. The distance from the center to a surface point measures the magnitude of the magnetization induced by a field spanning the given direction. The lobes correspond to the axes of easy magnetization of the i-th level. The maximal extension of the lobes of a given state can, in certain circumstances, be assimilated to the $|g_J J_z|$ amount.

Table 3 The results of CASSCF-SO calculations for the lowest levels of the $LnSc_2N@C_{80}$ complexes, with two different basis sets (6-31G and 6-31G*) on the fullerene fragment. The thirteen levels of the Ln = Tb case correspond to the LF split of the $^7F_6$ multiplet and the sixteen states for the Ln = Dy case are related to the $^6H_{15/2}$ term

Ln	Tb	Tb	Dy	Dy
Basis set on C	6-31G	6-31G*	6-31G	6-31G*
1	0.0	0.0	0.0	0.0
2	0.0	0.0	0.0	0.0
3	195.3	201.1	475.6	481.0
4	195.4	201.1	475.6	481.0
5	434.7	445.1	758.4	774.8
6	435.8	446.2	758.4	774.8
7	676.0	692.1	930.2	956.1
8	692.4	707.7	930.2	956.1
9	896.8	919.7	1059.2	1089.9
10	911.4	933.6	1059.2	1089.9
11	1026.5	1055.5	1171.3	1201.8
12	1105.4	1134.4	1171.3	1201.8
13	1130.5	1162.1	1247.0	1276.2
14			1247.0	1276.2
15			1346.1	1374.5
16			1346.1	1374.5

The zones similar to a nodal plane can be interpreted as matching directions with no response to the field perturbation. The $DySc_2NC_{80}$ system shows, in the lowest part of the spectrum, an axial pattern, having the magnetization lobes along the strongest LF line, *i.e.* the Ln–N bond. Besides, the maximal absolute values of the *ab initio* computed magnetization functions of the lowest couples are well matching the $|g_J J_z|$ pattern. The maximal extensions of the magnetization lobes for the lower couples, from {1, 2} to {9, 10}, correspond to the respective {9.95, 8.52, 7.20, 5.88, 4.36} μ_B values. These magnitudes are close to the {10.00, 8.67, 7.33, 6.00, 4.67} μ_B series, obtained with the ideal estimation by $g_J = 4/3$ and $J_z = \{\pm 15/2, \pm 13/2, \pm 11/2, \pm 9/2, \pm 7/2\}$ projections. A non-trivial result is that the anisotropy of the higher levels deviates from the axial pattern and shows lobes approximately placed in the Sc_2N plane (*i.e.* *xz* in our case).

In the case of upper states, the J_z is no longer a good quantum number, the magnetization polar map of the {11, 12} couple being a flattened ellipsoid, extended in the *xz* plane to a 2.79 μ_B radius. The {13, 14} and {15, 16} pairs show lobes with the 5.57 μ_B and 9.31 μ_B respective elongations along the *x* axis. The identification of the anisotropy pattern on each state, with respect to the molecular geometry, is a non-trivial issue, enabled by our methodology of further exploitation of the *ab initio* data, used to extract the response to the magnetic field perturbations.

The usual molecular magnetism deals merely with the ground state anisotropy. However, the pattern on the excited states is important as well, in fundamental respects, or in modelling the combined use of excitation and magnetic response, with relevance in possible future spintronics applications. The predicted details of the magnetic anisotropy and all the spectral states cannot be achieved properly without the full account of all the realistic LF effects and without the help of computation experiments in retrieving reasonable estimates, under conditions where experimental data cannot enable the whole parametric set. Note that the account of the magnetic anisotropy was done with data from the black box of the CASSCF-SO calculations, not by a treatment intermediated by the above extracted LF parameters, in the frame of a phenomenological modelling. In this way, the simulation includes the subtle effects that are not accounted in the classical LF modelling because of the mentioned holohedrization effect,[48] namely the lack of terms originating from the odd parity integrals, such

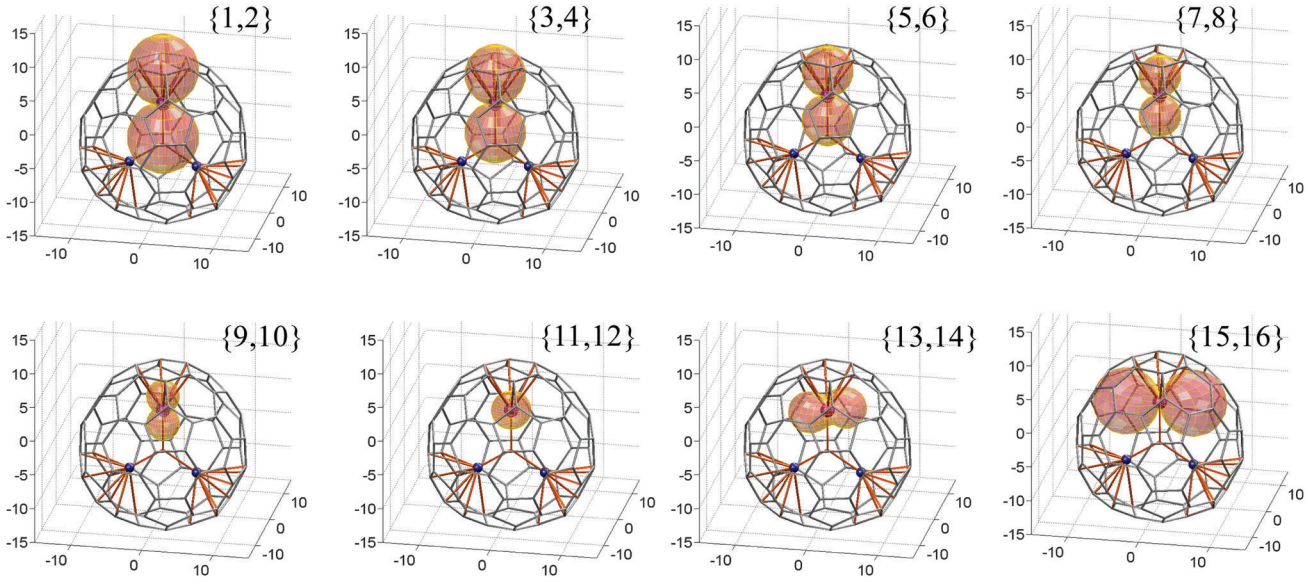

Fig. 3 Polar maps of the state-specific magnetization functions for the LF split components of the $J = 15/2$ multiplet, resulting from *ab initio* CASSCF-SO calculations. The diagrams for degenerate congeners are identical, labelling by $\{k, k+1\}$ the corresponding couples of states. The 3D frame in each panel corresponds to the $\{M_x, M_y, M_z\}$ components of magnetization per molecule (from -15 μ_B to $+15$ μ_B on each axis). The molecular skeleton is immersed at arbitrary scaling.

as the slight d–f mixing. Implementing, *a posteriori* to the *ab initio* calculations,[37] the explicit dependence of the magnetic field (as magnitude, B, and orientation, expressed by θ, φ polar angles of the vector) the sum of the state Z can be worked out:

$$Z(B,\theta,\varphi) = \sum_i \exp(-E_i(B,\theta,\varphi)/k_B T), \quad (4)$$

where E_i are the field-dependent eigenvalues of the CASSCF-SO calculations and k_B is the Boltzmann constant. The Z function is the basis for the *ab initio* simulation of the magnetic properties, taking the derivatives:

$$M(B,\theta,\varphi) = N_A k_B T \mathrm{d}\ln(Z(B,\theta,\varphi))/\mathrm{d}B, \quad (5)$$

$$\chi(B,\theta,\varphi) = N_A k_B T \mathrm{d}^2\ln(Z(B,\theta,\varphi))/\mathrm{d}B^2, \quad (6)$$

defining the anisotropic molar magnetization (M) and susceptibility (χ), respectively, along the direction specified by the θ and φ polar angles. In the above formulae, N_A is the Avogadro number. Considering that the molecules are oriented randomly in the sample, the averaged values are defined as follows:

$$\bar{M}(B) = (1/4\pi)\int_{\theta=0}^{\theta=\pi}\int_{\varphi=0}^{\varphi=2\pi} M(B,\theta,\varphi)\sin(\theta)\mathrm{d}\theta\mathrm{d}\varphi, \quad (7)$$

$$\bar{\chi}(B) = (1/4\pi)\int_{\theta=0}^{\theta=\pi}\int_{\varphi=0}^{\varphi=2\pi} \chi(B,\theta,\varphi)\sin(\theta)\mathrm{d}\theta\mathrm{d}\varphi. \quad (8)$$

The derivatives implied in formulae (3), (5) and (6) were estimated numerically, taking, a $\mathrm{d}B$ = 0.001 T increment and performing, *e.g.* the $Z(B, \theta, \varphi)$, $Z(B + \mathrm{d}B, \theta, \varphi)$ and $Z(B - \mathrm{d}B, \theta, \varphi)$, finite differences, necessary to estimate the first and second derivatives. The magnetic susceptibility is simulated at a small B = 0.1 T imposed field, in line with the usual experimental procedures. The integration assumed in formulae (7) and (8) was also considered numerically, taking the summation over a 24 × 48 grid of the θ, φ angles. The computed magnetization curves, at different temperatures and as a function of the magnetic field, averaged for all the space orientation are given in Fig. 4(a). One observes a reasonable match to the curves presented by Greber and collaborators in Fig. 3 from ref. 15. Note that the *ab initio* calculations cannot account for the complicated kinetic and mean-field lattice effects that determined the hysteretic version of the experimental magnetization curves, but fairly well reproduce the pattern and plateaus of the direct step, at increasing field. The averaging over all directions reduces the recorded curve, by a factor of about 1/2, in comparison to the anisotropic magnetization drawn along the z axis, $M(B, 0, 0)$, represented as inset in Fig. 4(a). The authors of the experimental report[15] inquired the possibility of LF reasons for the measured value (4.4 μ_B), if due to a groundstate with projection smaller than the $|J_z|$ = 15/2. Now, we can firmly state that the LF leads to a groundstate with maximal 15/2 projection, the lower plateaus being due to the averaged anisotropy, since other space orientations of the N–Dy axis lead to smaller induced magnetic moments, at the perturbation by a field fixed to a given direction. Since the random molecular orientation is frozen by intermolecular forces (van der Waals and electrostatic dipolar) stronger than the leverage of the magnetic field, the molecules are not realigned during the measurement.

To the best of our knowledge, the magnetic susceptibility was not yet measured for $DySc_2NC_{80}$ because of the scarcity of the samples. We present in Fig. 4(b) the computed χT *vs.* T curves waiting further experimental confirmation. The pattern of the computed curves is similar to those reported from anisotropic magnetic susceptibility on dysprosium complexes manifesting an effective strong axial ligand field.[49] The maximal plateau achieved by the χ_z susceptibility along the N–Dy axis is close to the ideal 37.5 value, estimated as $N_A(\mu_B \cdot g_J J_z)^2/k_B$, with g_J = 4/3 and J_z = ±15/2. In the cited experimental work on d–f complexes,[49] the low temperature part is modulated also by the

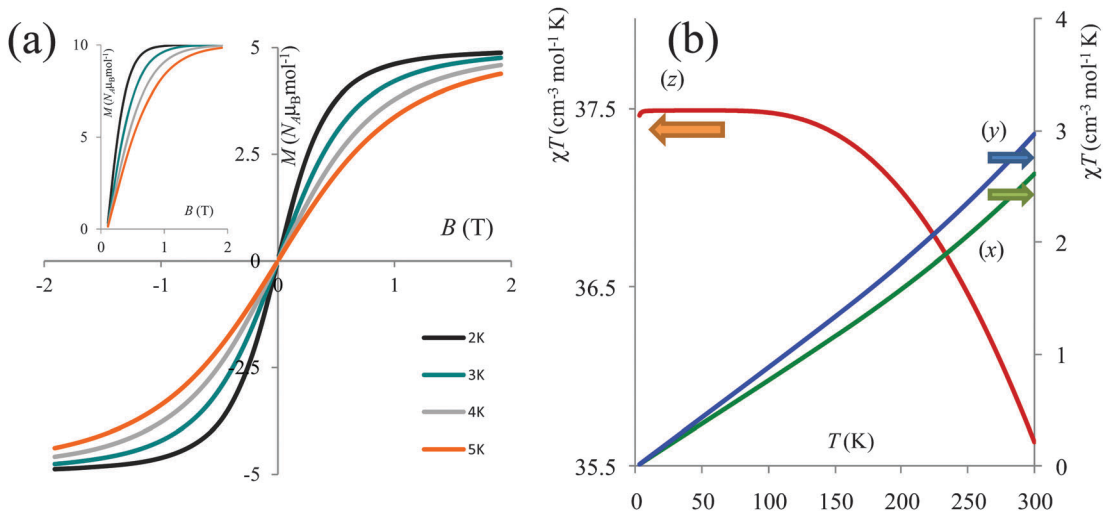

Fig. 4 (a) Computed magnetization curves, for various temperatures (T = 2–5 K) as a function of magnetic field (B = 0–2 Tesla). The curves are averages over the orientation disorder of molecular species. (b) Computed χT *vs.* T curves considered anisotropically along the x, y, and z axes. The z case is represented on the left-side axis, and x, y on the right-side.

exchange coupling with a Cu(II) ion, but the plateau due to the Dy(III) axial anisotropy is well visible. To be distinguished from the manifestations in coordination complexes, where the plateau extends to about 50 K, in our case the descending trend is simulated only after 100 K, as a consequence of stronger ligand field, which determined a larger separation of the $J_z = \pm 15/2$ and $J_z = \pm 13/2$ doublets.

Conclusions

Taking the $DySc_2NC_{80}$ endohedral fullerene with SIM behaviours as the prototype[15] case study for the electronic structure of the encapsulated lanthanide ion and the causal relationships with the special magnetic properties, we advanced methodological constructs and presented results that serve to explain the known experimental data and produce reliable predictions. Using the advents of our methodological outlines, previously tested in the field of molecular magnetism of lanthanide complexes,[25,37] we characterized the bonding regime of the lanthanide ion as obeying ligand field (LF) characteristics and extracted comprehensive lists of parameters from the state-of-the art *ab initio* calculations. Due to a short Dy–N distance, of about 2.2 Å (as compared to the usual ~2.4 Å range), cumulated with several Dy–C proximal (at about 2.6 Å) or more distant (~3.0 Å and larger) contacts, the resultant LF strength is higher than in usual lanthanide complexes. The system shows also a pronounced quasi-axial LF pattern that leads to the stabilization of a $J_z = \pm 15/2$ groundstate, as results from our CASSCF-SO (multi-configuration spin–orbit) calculations. The original idea of presenting polar maps taken from the derivative with respect to the magnetic field, from each state of the $J = 15/2$ multiplet, leads to a very clear description of the magnetic anisotropy in ground and excited states, adding a heuristic perspective to the quantitative technical account. The *ab initio* computed magnetization is in line with the experimental results, the outline of the simulated magnetic susceptibility preceding the yet unknown data. The *ab initio* approach is a valuable tool, allowing us to compensate, by thorough analysis and prediction, the scarcity of the experimental data, determined by the difficulty in obtaining sizeable samples.

Computational details

The multi-configuration quantum chemical computations and subsequent spin–orbit (SO) treatments were performed with the GAMESS program,[33] using the SBKJC[36] effective core potentials and basis sets for lanthanides, the 6-31G* basis set for the N and Sc atoms, and 6-31G or 6-31G* for the C atoms. For comparison purposes and NEVPT2 treatment[35] the ORCA[39] program was used. The molecular geometries were obtained from Density Functional Theory (DFT) optimization, carried out by means of the Amsterdam Density Functional (ADF) program package,[30] using triple zeta polarized basis sets (TZP) and the Becke–Perdew (BP86) functional.[50] The different codes were used in line with their specific capabilities. The ADF was chosen for the DFT step because the orbital control keywords allowed from the beginning obtaining f-type MOs in line with formal LF analysis purposes, a fact that is not accomplished in the usual DFT routines. The GAMESS was used for convenient handling of our non-standard procedures following the CASSCF-SO calculations, having easy access to data from the black-box of the calculations. The ORCA was used for the salient and efficient second order perturbation methods.

Acknowledgements

This work is supported by the UEFISC-CDI research grant PCE 14/2013 (Romania). Support from the Swiss National Science Foundation and the Swiss Secretariat for Innovation and Research is also acknowledged. W.U. thanks Dr Elena Sciaroni for financial support.

Notes and references

1 S. Cotton, *Lanthanide and actinide chemistry*, John Wiley & Sons, New York, 2006.
2 A. Hirsch and M. Brettreich, *Fullerenes: Chemistry and Reactions*, Wiley-VCH Verlag GmbH & Co. KGaA, Berlin, 2005.
3 M. M. Alvarez, E. G. Gillan, K. Holezer, R. B. Kaner, K. S. Min and R. L. Whetten, *J. Phys. Chem.*, 1991, **95**, 10561.
4 R. D. Johnson, M. S. de Vries, J. Salem, D. S. Bethune and C. S. Yannoni, *Nature*, 1992, **355**, 239.
5 (*a*) S. Hino, H. Takahashi, K. Iwasaki, K. Matsumoto, T. Miyazaki, S. Hasegawa, K. Kikuchi and Y. Achiba, *Phys. Rev. Lett.*, 1993, **71**, 4261; (*b*) R. A. J. Woolley, K. H. G. Schulte, L. Wang, P. J. Moriarty, B. C. C. Cowie, H. Shinohara, M. Kanai and T. J. S. Dennis, *Nano Lett.*, 2004, **4**, 361; (*c*) J. Q. Ding and S. H. Yang, *J. Am. Chem. Soc.*, 1996, **118**, 11254; (*d*) J. Q. Ding, N. Lin, L. T. Weng, N. Cue and S. H. Yang, *Chem. Phys. Lett.*, 1996, **261**, 92; (*e*) T. Okazaki, K. Suenaga, Y. F. Lian, Z. N. Gu and H. Shinohara, *J. Chem. Phys.*, 2000, **113**, 9593; (*f*) T. Okazaki, K. Suenaga, K. Hirahara, S. Bandow, S. Iijima and I. E. Shinohara, *J. Am. Chem. Soc.*, 2001, **123**, 9673; (*g*) H. J. Huang, S. H. Yang and X. X. Zhang, *J. Phys. Chem. B*, 2000, **104**, 1473; (*h*) H. J. Huang and S. H. Yang, *J. Organomet. Chem.*, 2000, **599**, 42; (*i*) H. J. Huang, S. H. Yang and X. X. Zhang, *J. Phys. Chem. B*, 1999, **103**, 5928.
6 E. G. Gillan, K. Yeretzian, K. S. Min, M. M. Alvarez, R. L. Whetten and R. B. Kaner, *J. Phys. Chem.*, 1992, **96**, 6869.
7 (*a*) T. Kanbara, Y. Kubozono, Y. Takabayashi, S. Fujiki, S. Iida, Y. Haruyama, S. Kashino, S. Emura and T. Akasaka, *Phys. Rev. B: Condens. Matter Mater. Phys.*, 2001, **64**, 113403; (*b*) T. Inoue, Y. Kubozono, S. Kashino, Y. Takabayashi, K. Fujitaka, M. Hida, M. Inoue, T. Kanbara, S. Emura and T. Uruga, *Chem. Phys. Lett.*, 2000, **316**, 381; (*c*) R. F. Sabirianov, W. N. Mei, J. Lu, Y. Gao, X. C. Zeng, R. D. Bolskar, P. Jeppson, N. Wu, A. N. Caruso and P. A. Dowben, *J. Phys.: Condens. Matter*, 2007, **19**, 6.
8 H. Shinohara, Endohedral Metallofullerenes, in *Fullerenes*, ed. K. M. Kadish and R. S. Ruoff, J. Wiley & Sons, New York, 2000, pp. 357–390.

9 A. Popov, S. Yang and L. Dunsch, *Chem. Rev.*, 2013, **113**, 5989.
10 X. Lu, Y. Lian, C. M. Beavers, N. Mizorogi, Z. Slanina, S. Nagase and T. Akasaka, *J. Am. Chem. Soc.*, 2011, **133**, 10772.
11 H. Yang, H. Jin, B. Hong, Z. Liu, C. M. Beavers, H. Zhen, Z. Wang, B. Q. Mercado, M. M. Olmstead and A. L. Balch, *J. Am. Chem. Soc.*, 2011, **133**, 16911.
12 W. Fu, J. Zhang, T. Fuhrer, H. Champion, K. Furukawa, T. Kato, J. E. Mahaney, B. G. Burke, K. A. Williams, K. Walker, C. Dixon, J. Ge, C. Shu, K. Harich and H. C. Dorn, *J. Am. Chem. Soc.*, 2011, **133**, 9741.
13 (*a*) A. Á. Náfrádi, Á. Pásztor, L. Forró, L. F. Kiss, T. Fehér, É. Kováts, S. Pekker and A. Jánossy, *J. Phys. Chem. Lett.*, 2012, **3**, 3291; (*b*) M. Treier, P. Ruffieux, R. Fasel, F. Nolting, S. Yang, L. Dunsch and T. Greber, *Phys. Rev. B: Condens. Matter Mater. Phys.*, 2009, **80**, 081403; (*c*) J. Tang, I. J. Hewitt, N. T. Madhu, G. Chastanet, W. Wernsdorfer, C. E. Anson, C. Benelli, R. Sessoli and A. K. Powell, *Angew. Chem., Int. Ed.*, 2006, **45**, 1729.
14 (*a*) M. M. Olmstead, A. de Bettencourt-Dias, J. C. Duchamp, S. Stevenson, H. C. Dorn and A. L. Balch, *J. Am. Chem. Soc.*, 2000, **122**, 12220; (*b*) L. Dunsch, M. Krause, J. Noack and P. Georgi, *J. Phys. Chem. Solids*, 2004, **65**, 309; (*c*) S. F. Yang, M. Kalbac, A. Popov and L. Dunsch, *ChemPhysChem*, 2006, 71990; (*d*) S. F. Yang, A. A. Popov, M. Kalbac and L. Dunsch, *Chem. – Eur. J.*, 2008, **14**, 2084; (*e*) S. Yang, A. A. Popov, C. Chen and L. Dunsch, *J. Phys. Chem. C*, 2009, **113**, 7616; (*f*) S. Stevenson, C. Chancellor, H. M. Lee, M. H. Olmstead and A. L. Balch, *Inorg. Chem.*, 2008, **47**, 1420.
15 R. Westerström, J. Dreiser, C. Piamonteze, M. Muntwiler, S. Weyeneth, H. Brune, S. Rusponi, F. Nolting, A. Popov, S. Yang, L. Dunsch and T. Greber, *J. Am. Chem. Soc.*, 2012, **134**, 9840.
16 (*a*) N. Ishikawa, M. Sugita, T. Okubo, N. Tanaka, T. Iino and Y. Kaizu, *Inorg. Chem.*, 2003, **42**, 2440; (*b*) N. Ishikawa, T. Iino and Y. Kaizu, *J. Phys. Chem. A*, 2002, **106**, 9543; (*c*) N. Ishikawa, M. Sugita and W. Wernsdorfer, *Angew. Chem., Int. Ed.*, 2005, **44**, 2931; (*d*) N. Ishikawa, M. Sugita and W. Wernsdorfer, *J. Am. Chem. Soc.*, 2005, **127**, 3650; (*e*) N. Ishikawa, *Struct. Bonding*, 2010, **135**, 211.
17 (*a*) G. Christou, D. Gatteschi, D. N. Hendrickson and R. Sessoli, *MRS Bull.*, 2000, **25**, 66; (*b*) D. Gatteschi and R. Sessoli, *Angew. Chem., Int. Ed.*, 2003, **42**, 268; (*c*) M. Murugesu, M. Habrych, W. Wernsdorfer, K. A. Abboud and G. Christou, *J. Am. Chem. Soc.*, 2004, **126**, 4766; (*d*) A. J. Tasiopoulos, A. Vinslava, W. Wernsdorfer, K. A. Abboud and G. Christou, *Angew. Chem.*, 2004, **116**, 2169; (*e*) G. Aromi and E. K. Brechin, *Struct. Bonding*, 2006, **122**, 1.
18 A. Caneschi, D. Gatteschi, R. Sessoli, A. L. Barra, L. C. Brunel and M. Guillot, *J. Am. Chem. Soc.*, 1991, **113**, 5873.
19 (*a*) K. R. Dunbar, *Inorg. Chem.*, 2012, **51**, 12055; (*b*) J.-P. Costes, F. Dahan and W. Wernsdorfer, *Inorg. Chem.*, 2006, **45**, 5.
20 D. Aravena and E. Ruiz, *Inorg. Chem.*, 2013, **52**, 13770.
21 (*a*) R. Sessoli, D. Gatteschi, A. Caneschi and M. Novak, *Nature*, 1993, **365**, 141; (*b*) M. N. Leuenberger and D. Loss, *Nature*, 2001, **410**, 789; (*c*) L. Bogani and W. Wernsdorfer, *Nat. Mater.*, 2008, **7**, 179.
22 W. Andreoni and A. Curioni, Theory of Endohedraly Doped Fullerene, in *The Chemical Physics of Fullerenes*, ed. W. Andreoni, 1996, Kluwer, Dordrecht, pp. 183–196.
23 J. Lu, X. Zhang, X. Zhao, S. Nagase and K. Kobayashi, *Chem. Phys. Lett.*, 2000, **332**, 219.
24 W. Koch and M. C. Holthausen, *A Chemist's Guide to Density Functional Theory*, Wiley-VCH, Berlin, 2001.
25 (*a*) J. Paulovic, F. Cimpoesu, M. Ferbinteanu and K. Hirao, *J. Am. Chem. Soc.*, 2004, **126**, 3321; (*b*) M. Ferbinteanu, T. Kajiwara, K.-Y. Choi, H. Nojiri, A. Nakamoto, N. Kojima, F. Cimpoesu, Y. Fujimura, S. Takaishi and M. Yamashita, *J. Am. Chem. Soc.*, 2006, **128**, 9008.
26 (*a*) M. Zbiri, C. Daul and T. A. Wesolowski, *J. Chem. Theory Comput.*, 2006, **2**, 1106; (*b*) A. Borel, L. Helm and C. Daul, *Chem. Phys. Lett.*, 2004, **383**, 584; (*c*) M. Zbiri, M. Atanasov, C. Daul, J. M. Garcia-Lastra and T. A. Wesolowski, *Chem. Phys. Lett.*, 2004, **397**, 441; (*d*) M. Atanasov, C. Daul, H. U. Güdel, T. A. Wesolowski and M. Zbiri, *Inorg. Chem.*, 2005, **44**, 2954.
27 (*a*) M. Atanasov, C. Daul and C. Rauzy, *Chem. Phys. Lett.*, 2003, **367**, 737; (*b*) C. Daul, *Int. J. Quantum Chem.*, 1994, **52**, 867; (*c*) T. Minerva, A. Goursot and C. Daul, *Chem. Phys. Lett.*, 2001, **350**, 147.
28 (*a*) H. Ramanantoanina, W. Urland, F. Cimpoesu and C. Daul, *Phys. Chem. Chem. Phys.*, 2013, **15**, 13902; (*b*) H. Ramanantoanina, W. Urland, A. García-Fuente, F. Cimpoesu and C. Daul, *Chem. Phys. Lett.*, 2013, **588**, 260.
29 (*a*) E. K. U. Gross, L. N. Oliveria and W. Kohn, *Phys. Rev. A: At., Mol., Opt. Phys.*, 1988, **37**, 2809; (*b*) C. A. Ullrich and W. Kohn, *Phys. Rev. Lett.*, 2001, **87**, 093001; (*c*) E. Cances, *J. Chem. Phys.*, 2001, **114**, 10616.
30 (*a*) ADF2012.01, SCM, Theoretical Chemistry, Vrije Universiteit, Amsterdam, The Netherlands, http://www.scm.com; (*b*) G. te Velde, F. M. Bickelhaupt, S. J. A. van Gisbergen, C. Fonseca Guerra, E. J. Baerends, J. G. Snijders and T. Ziegler, *J. Comput. Chem.*, 2001, **22**, 931; (*c*) C. Fonseca Guerra, J. G. Snijders, G. te Velde and E. J. Baerends, *Theor. Chem. Acc.*, 1998, **99**, 391.
31 (*a*) T. A. Wesolowski and A. Warshel, *J. Phys. Chem.*, 1993, **97**, 8050; (*b*) J. Neugebauer, C. R. Jacob, T. A. Wesolowski and E. J. Baerends, *J. Phys. Chem. A*, 2005, **109**, 7805.
32 (*a*) A. De Cian, M. Moussavi, J. Fischer and R. Weiss, *Inorg. Chem.*, 1985, **24**, 3162; (*b*) M. Moussavi, A. De Cian, J. Fischer and R. Weiss, *Inorg. Chem.*, 1988, **27**, 1287.
33 M. W. Schmidt, K. K. Baldridge, J. A. Boatz, S. T. Elbert, M. S. Gordon, J. H. Jensen, S. Koseki, N. Matsunaga, K. A. Nguyen, S. J. Su, T. L. Windus, M. Dupuis and J. A. Montgomery, *J. Comput. Chem.*, 1993, **14**, 1347.
34 (*a*) K. Hirao, *Chem. Phys. Lett.*, 1992, **190**, 374; (*b*) H. Nakano, K. Nakayama, K. Hirao and M. Dupuis, *J. Chem. Phys.*, 1997, **106**, 4912; (*c*) H. Nakano, *J. Chem. Phys.*, 1993, **99**, 7983; (*d*) K. Andersson, P.-Å. Malmqvist, B. O. Roos, A. J. Sadlej and K. Wolinski, *J. Phys. Chem.*, 1990, **94**, 5483; (*e*) B. O. Roos, K. Andersson, M. K. Fulscher, P.-A. Malmqvist, L. Serrano-Andres, K. Pierloot and M. Merchan, *Adv. Chem. Phys.*, 1996, **93**, 219; (*f*) K. Pierloot, in *Computational Organometallic*

Chemistry, ed. T. Cundari, Marcel Dekker Inc., New York, 2001, pp. 123–158.

35 (*a*) C. Angeli, R. Cimiraglia, S. Evangelisti, T. Leininger and J.-P. Malrieu, *J. Chem. Phys.*, 2001, **114**, 10252; (*b*) C. Angeli, R. Cimiraglia and J.-P. Malrieu, *J. Chem. Phys.*, 2002, **117**, 9138; (*c*) C. Angeli, B. Bories, A. Cavallini and R. Cimiraglia, *J. Chem. Phys.*, 2006, **124**, 054108.

36 (*a*) W. J. Stevens, H. Basch and M. Krauss, *J. Chem. Phys.*, 1984, **81**, 6026; (*b*) W. J. Stevens, M. Krauss, H. Basch and P. G. Jasien, *Can. J. Chem.*, 1992, **70**, 612; (*c*) T. R. Cundari and W. J. Stevens, *J. Chem. Phys.*, 1993, **98**, 5555.

37 (*a*) M. Ferbinteanu, F. Cimpoesu, M. A. Gîrtu, C. Enachescu and S. Tanase, *Inorg. Chem.*, 2012, **51**, 40; (*b*) F. Cimpoesu, S. Dahan, S. Ladeira, M. Ferbinteanu and J.-P. Costes, *Inorg. Chem.*, 2012, **51**, 11279.

38 (*a*) J. Ivanic and K. Ruedenberg, *Theor. Chem. Acc.*, 2001, **106**, 339; (*b*) J. Ivanic, *J. Chem. Phys.*, 2003, **119**, 9364; (*c*) L. Roskop and M. S. Gordon, *J. Chem. Phys.*, 2012, **135**, 044101.

39 F. Neese, *ORCA-an ab initio, Density Functional and Semiempirical program package*, Max-Planck Institute for Energie Conversion, Mülheim an der Ruhr, Germany, 2013.

40 D. A. Pantazis and F. Neese, *J. Chem. Theory Comput.*, 2009, **5**, 2229.

41 (*a*) A. J. Freeman and R. E. Watson, *Phys. Rev.*, 1962, **127**, 2058; (*b*) S. Hüfner, *Optical Spectra of Transparent Rare Earth Compounds*, Academic Press, New York, 1978.

42 D. J. Newman and B. Ng, *Crystal Field Handbook*, Cambridge University Press, Cambridge, 2000.

43 (*a*) D. J. Newman and G. Stedman, *J. Chem. Phys.*, 1969, **51**, 3013; (*b*) D. J. Newman and B. Ng, *J. Phys.: Condens. Matter*, 1989, **1**, 1613; (*c*) D. J. Newman and B. Ng, *Rep. Prog. Phys.*, 1989, **52**, 699.

44 (*a*) W. Urland, *Chem. Phys.*, 1976, **14**, 393; (*b*) W. Urland, *Chem. Phys. Lett.*, 1977, **46**, 457; (*c*) W. Urland, *Chem. Phys. Lett.*, 1981, **77**, 58; (*d*) W. Urland, *Chem. Phys. Lett.*, 1981, **83**, 116.

45 (*a*) W. Urland and R. Kremer, *Inorg. Chem.*, 1984, **23**, 1550; (*b*) S. T. Hatscher and W. Urland, *J. Solid State Chem.*, 2003, **176**, 288; (*c*) F. Soetebier and W. Urland, *Eur. J. Inorg. Chem.*, 2002, 1673.

46 B. G. Wybourne, *Spectroscopic Properties of Rare Earths*, Wiley Interscience, New York, 1965.

47 K. W. H. Stevens, *Proc. Phys. Soc., London, Sect. A*, 1952, **65**, 209.

48 (*a*) C. F. Schäffer, *Proc. R. Soc. A*, 1967, **297**, 96; (*b*) C. F. Schäffer, *Theor. Chim. Acta*, 1966, **4**, 166.

49 T. Kajiwara, M. Nakamo, K. Takahashi, S. Takaishi and M. Yamashita, *Chem. – Eur. J.*, 2011, **17**, 196.

50 (*a*) A. D. Becke, *Phys. Rev. A: At., Mol., Opt. Phys.*, 1988, **38**, 3098; (*b*) J. P. Perdew, *Phys. Rev. B: Condens. Matter Mater. Phys.*, 1986, **33**, 8822; (*c*) J. P. Perdew, *Phys. Rev. B: Condens. Matter Mater. Phys.*, 1986, **34**, 7406.

